TU Delft

Delft University of Technology

Accelerated Life Test and Prediction of Electromigration in Aluminum Interconnects coupling Multiphysics Full Coupled Model with Optimized Atomic Flux Divergence Simulation

Wang, Xueliang; Feng, Shuo; Luo, Tao; Zhang, Jinyuan; Zhang, Yaqian; Fan, Xuejun; Zhang, Guoqi; Fan, Jiajie

DOI
10.1109/TCPMT.2025.3554259

Publication date
2025

Document Version
Final published version

Published in
IEEE Transactions on Components, Packaging and Manufacturing Technology

Citation (APA)
Wang, X., Feng, S., Luo, T., Zhang, J., Zhang, Y., Fan, X., Zhang, G., & Fan, J. (2025). Accelerated Life Test and Prediction of Electromigration in Aluminum Interconnects coupling Multiphysics Full Coupled Model with Optimized Atomic Flux Divergence Simulation. *IEEE Transactions on Components, Packaging and Manufacturing Technology*, *15*(5), 949-958. https://doi.org/10.1109/TCPMT.2025.3554259

Important note
To cite this publication, please use the final published version (if applicable).
Please check the document version above.

Copyright
Other than for strictly personal use, it is not permitted to download, forward or distribute the text or part of it, without the consent of the author(s) and/or copyright holder(s), unless the work is under an open content license such as Creative Commons.

Takedown policy
Please contact us and provide details if you believe this document breaches copyrights.
We will remove access to the work immediately and investigate your claim.

Green Open Access added to TU Delft Institutional Repository

'You share, we take care!' - Taverne project

https://www.openaccess.nl/en/you-share-we-take-care

Otherwise as indicated in the copyright section: the publisher is the copyright holder of this work and the author uses the Dutch legislation to make this work public.

Accelerated Life Test and Prediction of Electromigration in Aluminum Interconnects Coupling Multiphysics Full Coupled Model With Optimized Atomic Flux Divergence Simulation

Xueliang Wang, Shuo Feng, Tao Luo, Jinyuan Zhang, Yaqian Zhang, Zhen Cui, Xuejun Fan, *Fellow, IEEE*, Guoqi Zhang, *Fellow, IEEE*, and Jiajie Fan, *Senior Member, IEEE*

***Abstract*—With the miniaturization and high-power requirements of microelectronic devices, the current density carried by interconnects in packaging structures continually increases and reaches the threshold of electromigration (EM) failure. In this study, we investigated the microstructure evolution and void formation in aluminum (Al) interconnects during EM at three different current densities (1/3/5 MA/cm^2) and proposed a method coupling the fully coupled theory with an optimized atomic flux divergence method. The results show as follows. First, for the interconnects in integrated circuits, current density is the main factor affecting the EM lifetime of the interconnects in a certain temperature range. With the gradual increase of current density, the contribution of thermal transfer on EM cannot be ignored. The atomic concentration gradient and stress gradient can inhibit EM failure. Second, the increase of length and the decrease of width of interconnect will lead to the increase of atomic flux inside the structure, resulting in the accumulation of voids and atoms. Third, the structure is dynamically reconstructed after deleting the atoms below the failure threshold and the simulation results agree well with the experimental results. Compared with the traditional atomic flux divergence method, the improved atomic flux divergence method based on the fully coupled theory can better fit the change trend of atomic concentration after interconnect failure, and the failure time error is reduced by about 10%.**

***Index Terms*—Accelerated life prediction, aluminum interconnect, atomic flux divergence method, electromigration (EM), multiphysics simulation.**

Received 22 October 2024; revised 3 March 2025; accepted 15 March 2025. Date of publication 26 March 2025; date of current version 8 May 2025. This work was supported by the National Natural Science Foundation of China under Grant 52275559 and in part by Shanghai Pujiang Program under Grant 2021PJD002. Recommended for publication by Associate Editor C. Bailey upon evaluation of reviewers' comments. *(Xueliang Wang and Shuo Feng contributed equally to this work.) (Corresponding author: Jiajie Fan.)*

Xueliang Wang, Shuo Feng, Tao Luo, and Jinyuan Zhang are with Shanghai Engineering Technology Research Center of SiC Power Device, Academy for Engineering and Technology, Fudan University, Shanghai 200433, China (e-mail: 23210860006@m.fudan.edu.cn; 21210860045@m.fudan.edu.cn; 23210720219@m.fudan.edu.cn; 23210720130@m.fudan.edu.cn).

Yaqian Zhang, Zhen Cui, and Guoqi Zhang are with the EEMCS Faculty, Delft University of Technology, 2628 Delft, The Netherlands (e-mail: y.zhang-37@tudelft.nl; z.cui@tudelft.nl; G.Q.Zhang@TUDelft.nl).

Xuejun Fan is with the Department of Mechanical Engineering, Lamar University, Beaumont, TX 77710 USA (e-mail: xfan@lamar.edu).

Jiajie Fan is with Shanghai Engineering Technology Research Center of SiC Power Device, Academy for Engineering and Technology, Fudan University, Shanghai 200433, China, and also with the Research Institute of Fudan University in Ningbo, Ningbo 315336, China (e-mail: jiajie_fan@fudan.edu.cn).

Digital Object Identifier 10.1109/TCPMT.2025.3554259

I. Introduction

HIGH-DENSITY microelectronic packaging technologies are rapidly developing [1], [2], [3]. Represented by ball grid array (BGA) packaging, chip scale packaging (CSP), and heterogeneous packaging, high-density microelectronic packaging technologies enable higher interconnect performance with lower-power SiC [4], [5], [6]. However, the device size reduction has inevitably led to a higher-current density, which increases the performance burden of the package power supply module and exceeds its allowable limit (the order of magnitude of current density increases from 10^4 to 10^5 A/cm^2, or even larger) [7], [8], [9], and the load situation becomes more complicated, which can easily lead to serious electromigration (EM) failure, threatening the reliability of interconnects. Therefore, EM continues to be a topic of considerable interest for microelectronic reliability [10], [11].

EM is an enhanced mass transport process dominated by high-current density and coupled by multiple driving forces, which causes metal atoms to diffuse along the opposite direction of current [12], [13]. Although EM is a failure caused by high-current density, it cannot be considered that current density is the sole or dominant influencing factor of EM failure. Blech and Tai [14], Blech and Herring [15], and Blech [16] published a series of papers reporting on the scale effect of EM failure, which meant that EM failure could no longer be observed when the length of the wire was less than a certain critical value. Blech suggested that the stress gradient generated during EM balanced the electron wind force and hindered the occurrence of EM. Thereafter, Korhonen et al. [17] connected the rate of stress generation to EM. A model proposed by Korhonen et al. [17] for the evolution of stress in confined metal interconnects due to EM effects was later refined and completed by Clement and Thompson [18]. Besides, the EM-induced stress buildup at a blocking boundary was presented. Clement and Thompson [18] proposed the potential for maximum hydrostatic stress to

2156-3950 © 2025 IEEE. All rights reserved, including rights for text and data mining, and training of artificial intelligence and similar technologies. Personal use is permitted, but republication/redistribution requires IEEE permission.
See https://www.ieee.org/publications/rights/index.html for more information.

Authorized licensed use limited to: TU Delft Library. Downloaded on June 02,2025 at 10:30:01 UTC from IEEE Xplore. Restrictions apply.

arise in the interconnect, leading to void nucleation. Following this, Sarychev et al. [19] furthered this understanding by introducing a set of 3-D equations to model stress evolution during EM processes. Their approach incorporated the constitutive equation and stress equilibrium equation to comprehend the mechanism. Both these studies concurred that EM failure was essentially a mechanical phenomenon resulting from stress exceeding the material's tolerable limits. Notably, classical nucleation theory predicts that bulk void formation in aluminum interconnects requires overcoming a high-energy barrier. However, experiments observe rapid void nucleation under low-stress conditions, suggesting alternative low-energy pathways. Gleixner et al.'s [20] atomistic simulations reveal that nanoscale defects can directly induce void nucleation under typical process stresses without requiring long-term thermal equilibrium. This work establishes a critical link between defect-driven nucleation at the atomic scale and macroscopic EM failure patterns observed experimentally.

In the article published by Cui et al. [21], a general coupling model of EM was established, and the calculation results showed that self-migration caused by concentration gradients might play a more important role in hindering EM than stress gradients. At the same time, this article proposed diffusion strain, established a self-consistent constitutive equation, and explained that the commonly used Narro–Herry equation might overestimate the magnitude of stress and exaggerate the effect of stress gradients. Afterward, Cui et al. [22] obtained the diffusion strain coefficient through molecular dynamics simulation, and the simulation results were consistent with the experiment. This article also fundamentally explained the relationship between vacancy concentration, atomic concentration, and hydrostatic pressure under the condition of fully constrain. Recently, Cui et al. [23] reported the role of thermal migration induced by temperature gradient in EM; through the experiment, the author observed the spreading of voids in the middle region of conductors under the elevated current densities of 3 and 5 MA/cm^2. Through 1-D numerical simulation based on a fully coupled model, the author found that temperature gradient caused by different current densities were the dominant factors leading to EM failure.

In this article, the EM failure of standard wafer-level EM acceleration test (SWEAT)-like structures under different current densities based on previous testing platforms and theoretical models was further explored. First, a simulation method for accelerating the EM of electronic devices under 3-D multiphysical field coupling was proposed. In the experiment, an accelerated EM experimental platform was built to monitor the resistance of the interconnect with time. The EM failure position along the current direction and the atomic accumulation and diffusion mechanism was analyzed. Then, using the finite element calculation method (FEM) and based on the traditional atomic flux divergence method, a simulation method of EM acceleration of electronic devices under 3-D multiphysical field coupling was proposed to quantitatively analyze the contribution of current density, temperature, stress, and self-diffusion to EM. Finally, the function of atomic concentration and interconnect resistivity was derived, and the experimental results were compared with the simulation results. The remainder of this article is organized as follows. Section II introduces the EM test sample preparation and accelerated life test setup. The theoretical model and simulations details are described in Section III. The factors affecting EM and lifetime prediction are discussed in Section IV. Finally, Section V provides concluding remarks.

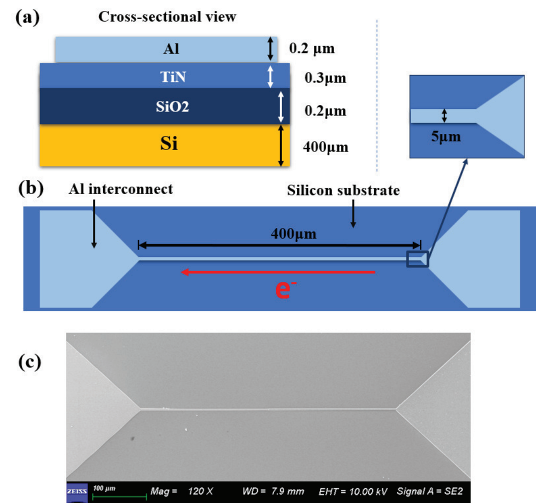

Fig. 1. (a) Illustration of the stacking layer of EM test sample. (b) SWEAT-like structure. (c) Scanning electron microscope (SEM) picture of 400 μm SWEAT structure.

II. EM Test Sample Preparation and Accelerated Life Test Setup

This section outlines the preparation process of EM test samples, and then introduces the composition of the experimental platform for EM accelerated testing.

A. Sample Preparation

Fig. 1(a) shows the stacking layer structure of EM test sample. The sample fabrication began with growing 200-nm-thick SiO_2 by thermal oxidation on a silicon wafer as an etching stopping layer and a thermally isolated layer. Then, a 300-nm-thick titanium nitride (TiN) layer was deposited on the SiO_2 layer by sputtering. During this procedure, the reactive gas (N_2) and vapor-phase titanium underwent a reaction within the vacuum chamber, resulting in the formation of TiN. Notably, even at room temperature (25 °C), an oxidation layer tends to develop on the surface of the TiN layer. Consequently, a hot sputter etch (HSE) process was implemented to eliminate this oxide layer. Following this step, a 200-nm-thick Al layer was deposited onto the TiN surface using reactive sputtering at 300 °C. Subsequently, the desired SWEAT structure was achieved through wet etching, which involved the creation of a narrow Al line connected to two large pads positioned on either side [as illustrated in Fig. 1(b)] [22].

B. Accelerated Life Test Setup

Fig. 2 depicts a schematic representation of the accelerated EM life test setup. The core component of this experimental configuration is the Nextron MPS-CHH microprobe

Authorized licensed use limited to: TU Delft Library. Downloaded on June 02,2025 at 10:30:01 UTC from IEEE Xplore. Restrictions apply.

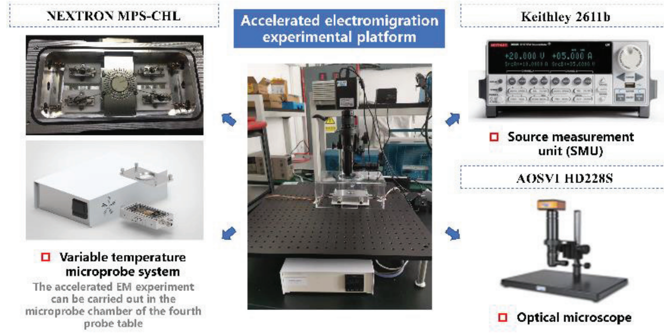

Fig. 2. Accelerated EM life test platform.

chamber, originating from Busan city, South Korea, which features a ceramic chuck. This chamber is designed to achieve vacuum conditions, enabling electrical measurements to be conducted using four probe needles, each tipped with 20-μm rhodium. Beneath the ceramic chuck, a temperature controller is installed, allowing for precise temperature adjustment ranging from 50 °C to 500 °C. Moreover, a source measurement unit (Keithley 2611b) and optical microscope (AOSVI HD228S) were included to in situ monitor the changes in electrical resistances and observe the evolution of the sample morphology.

III. Theoretical Model and Simulations

In this section, the multiphysics fully coupled theory of EM is introduced. Subsequently, an EM simulation method based on an improved atomic flux method is proposed and the simulation parameter setting is finally presented.

A. Multiphysics Fully Coupled Theory

According to Fick's first law, the change in atomic concentration in the EM process always obeys the conservation of mass equation, and the total mass of atoms remains unchanged in the EM process [24]. The time-dependent evolution equation of the local atomic concentration used in our atomic diffusion model is described by the following equation [25]:

$$\frac{\partial C}{\partial t} + \nabla \cdot \boldsymbol{J} = 0 \tag{1}$$

where C (m^{-3}) is the normalized atomic concentration $C = C_{\mathrm{a}}/C_{\mathrm{a}0}$, C_{a} is the atomic concentration, and $C_{\mathrm{a}0}$ is the initial atomic concentration. Then, t(s) is the time, and $\boldsymbol{J}$ (m^2/s) is the total atomic current density.

The overall atomic diffusion flux comprises the cumulative effects of atomic fluxes stemming from various driving forces. Specifically, the total atomic migration flux induced by the electron wind, thermal gradient, stress gradient, and atomic concentration gradient can be mathematically expressed as follows [16]:

$$\boldsymbol{J} = \boldsymbol{J}_E + \boldsymbol{J}_{\mathrm{TM}} + \boldsymbol{J}_s + \boldsymbol{J}_c \tag{2}$$

where $\boldsymbol{J}_E$ is the flux of EM atoms caused by the electron wind, the combined force of the electrostatic force, and the electron wind force of metal ions in an electric field. Thus, the uneven current produces uneven Joule heat distribution, and atoms in the interconnect diffuse and migrate along the temperature gradient, causing heat migration $\boldsymbol{J}_{\mathrm{TM}}$. $\boldsymbol{J}_s$ is driven by the electron wind; atoms diffuse from the cathode to the anode, and many atoms accumulate in the anode to form compressive stress. The cathode forms tensile stress, creating a stress gradient from the anode to the cathode. Under the combined action of the electron wind, temperature gradient, and stress gradient, the interconnected atoms diffuse and rearrange, resulting in an uneven atomic concentration distribution [26], [27]. The atomic concentration in the diffusion region decreases, and the atomic concentration increases in the diffusion accumulation region, resulting in the atomic concentration gradient $\boldsymbol{J}_c$.

The equations of $\boldsymbol{J}_E, \boldsymbol{J}_{\mathrm{TM}}, \boldsymbol{J}_s, \boldsymbol{J}_c$ are given below [28], [29]

$$\boldsymbol{J}_E = \frac{C_{\mathrm{a}}D_{\mathrm{a}}}{kT}eZ^*E = \frac{C_{\mathrm{a}}D_{\mathrm{a}}}{kT}eZ^*\rho j \tag{3}$$

$$\boldsymbol{J}_{\mathrm{TM}} = \frac{C_{\mathrm{a}}D_{\mathrm{a}}}{kT^2}Q^*\nabla T \tag{4}$$

$$\boldsymbol{J}_s = -\frac{C_{\mathrm{a}}D_{\mathrm{a}}}{kT}\Omega\nabla\sigma \tag{5}$$

$$\boldsymbol{J}_c = -D_{\mathrm{a}}\nabla C_{\mathrm{a}}. \tag{6}$$

According to phenomenological theory, the total flux of migrating atoms under multiphysics coupling is the sum of atomic fluxes caused by multiple driving forces. Thus, the expression of regularized total flux can be written as follows:

$$\begin{aligned}\boldsymbol{J} &= \boldsymbol{J}_E + \boldsymbol{J}_{\mathrm{TM}} + \boldsymbol{J}_s + \boldsymbol{J}_c \\ &= \frac{C_{\mathrm{a}}D_{\mathrm{a}}}{kT}eZ^*\rho j + \frac{C_{\mathrm{a}}D_{\mathrm{a}}}{kT^2}Q^*\nabla T - \frac{C_{\mathrm{a}}D_{\mathrm{a}}}{kT}\Omega\nabla\sigma - D_{\mathrm{a}}\nabla C_{\mathrm{a}}.\end{aligned} \tag{7}$$

The atomic concentration can be obtained at any time by combining (1) with (2). It is transformed into a coefficient partial differential equation as follows:

$$\begin{aligned}&\frac{\partial C}{\partial t} + \nabla \cdot \left\{\frac{C_{\mathrm{a}}D_{\mathrm{a}}}{kT}\left(eZ^*\rho j - \frac{\nabla T}{T}Q^* + \Omega\nabla\sigma\right)\right\} \\ &\quad - D_{\mathrm{a}}\nabla^2 C_{\mathrm{a}} = 0.\end{aligned} \tag{8}$$

In general, on the boundary of the metal interconnect, the boundary condition of the EM evolution equation can be expressed as

$$\boldsymbol{J} \cdot \boldsymbol{n} = 0_{\mathrm{on}}\Gamma. \tag{9}$$

Initial conditions (for all nodes):$C_{\mathrm{a}0} = 1$.

B. Improved Atomic Flux Method

Electrothermal coupling simulations can only obtain the distribution of current density and temperature gradient in the interconnect. Determining the EM failure location by the position of the maximum current density is not accurate, and various migration mechanisms will affect the atomic flux in the interconnect. In this part, the atomic flux divergence method is introduced to describe the EM process by the divergence of the electron wind, temperature gradient, and stress gradient, which are the main driving forces of EM. The atomic flux divergence distribution in the structure and its failure time were calculated. The position of the maximum atomic flux divergence is the weakest part of the metal interconnect, and it will be the place where the void failure occurs first [29].

Authorized licensed use limited to: TU Delft Library. Downloaded on June 02,2025 at 10:30:01 UTC from IEEE Xplore. Restrictions apply.

The flux component of the atomic density gradient is usually ignored in the traditional atomic flux divergence method; that is, the total atomic flux is simplified as follows:

$$\boldsymbol{J} = \boldsymbol{J}_E + \boldsymbol{J}_{\mathrm{TM}} + \boldsymbol{J}_s = \frac{C_{\mathrm{a}} D_{\mathrm{a}}}{kT} e Z^* \rho j + \frac{C_{\mathrm{a}} D_{\mathrm{a}}}{kT^2} Q^* \nabla T - \frac{C_{\mathrm{a}} D_{\mathrm{a}}}{kT} \Omega \nabla \sigma. \quad (10)$$

In order to provide a clearer description of the stacking or loss of atoms, we introduce the atomic flux divergence method. Assuming that the current density j is constant, the atomic flux divergence caused by the electron wind is as follows:

$$\operatorname{div}(\boldsymbol{J}_E) = \left(\frac{E}{kT} - \frac{1}{T} + \frac{\rho_0}{\rho}\right) \cdot \boldsymbol{J}_E \cdot \nabla T + \frac{\boldsymbol{J}_E}{C_{\mathrm{a}}} \cdot \nabla C_{\mathrm{a}}. \quad (11)$$

The atomic flux divergence caused by the temperature gradient is as follows [30]:

$$\operatorname{div}(\boldsymbol{J}_{\mathrm{TM}}) = \left(\frac{E}{kT} - \frac{2}{T}\right) \cdot \boldsymbol{J}_{\mathrm{TM}} \cdot \nabla T - \frac{C_{\mathrm{a}} D_{\mathrm{a}}}{kT} Q^* \operatorname{div}(\nabla T) + \frac{\boldsymbol{J}_{\mathrm{TM}}}{C_{\mathrm{a}}} \cdot \nabla C_{\mathrm{a}}. \quad (12)$$

The divergence of atomic flux caused by the stress gradient is as follows:

$$\operatorname{div}(\boldsymbol{J}_s) = \left(\frac{E}{kT} - \frac{1}{T}\right) \cdot \boldsymbol{J}_s \cdot \nabla T - \frac{C_{\mathrm{a}} D_{\mathrm{a}}}{kT} Q^* \operatorname{div}(\nabla \sigma) + \frac{\boldsymbol{J}_s}{C_{\mathrm{a}}} \cdot \nabla C_{\mathrm{a}}. \quad (13)$$

In summary, the total atomic flux divergence caused by the electron wind, temperature gradient, and stress gradient is as follows [31]:

$$\operatorname{div}(\boldsymbol{J}) = \operatorname{div}(\boldsymbol{J}_E) + \operatorname{div}(\boldsymbol{J}_{\mathrm{TM}}) + \operatorname{div}(\boldsymbol{J}_s) = C_{\mathrm{a}} \cdot F(T, \sigma, j, \ldots) + (\nabla C_{\mathrm{a}}) \cdot G(T, \sigma, j, \ldots). \quad (14)$$

The F and G functions are composed of different physical parameters plus the atomic concentration divergence. Substituting (14) into (10) and based on the explicit Euler equation, we can obtain the following:

$$C_{i+1} = C_i e^{-F_i \Delta t_i} - \Delta t_i (\nabla C_{\mathrm{a}})_i \cdot G_i \quad (15)$$

where C_i is the atomic concentration at initial step, F_i is the F function at initial step, and G_i is the G function at initial step.

The comparison between the improved atomic flux divergence method proposed in this article and previous studies is shown in Table I.

The above derivation shows that the atomic flux divergence method neglects the effects of atomic density flux $\boldsymbol{J}_c$. This article examines the impact of atomic density flux on EM using the traditional atomic flux divergence method to quantitatively analyze the influence of various driving forces.

TABLE I
SUMMARY OF SEVERAL PREVIOUS STUDIES

Models	Self-diffusion	Thermo-migration	Constraint condition	Stress equilibrium	Lifetime prediction
Sasagawa [32]	×	×	×	√	×
Tan [33]	√	√	×	×	√
Zhao [34]	√	√	×	√	×
Guan[35]	√	√	√	×	×
Improved Atomic Flux Method	√	√	√	√	√

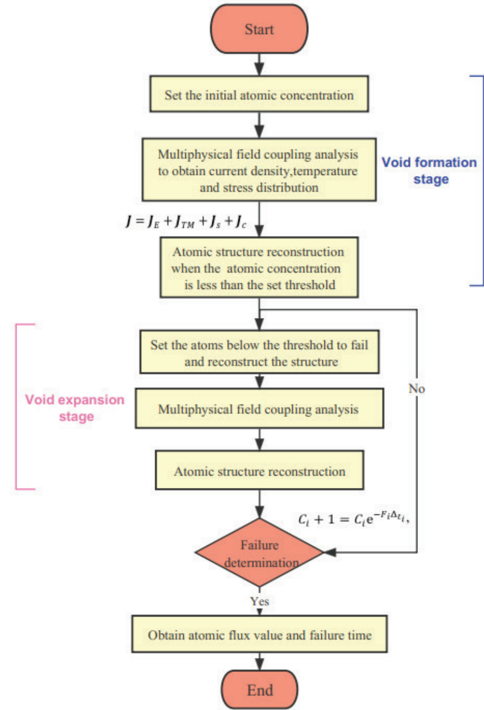

Fig. 3. Flowchart of EM simulation procedure.

C. EM Simulation Procedure and Parameter Setting

To simulate EM failure in interconnects under actual working conditions, we performed a multiphysics coupled steady-state analysis using COMSOL. In this study, EM failure is divided into two stages: void formation and void expansion. We obtained the distributions of current density, temperature, and structural stress prior to failure and combined these with an analysis of atomic diffusion. Whenever the average atomic concentration of atoms in the structure reached the failure threshold $(C_{\mathrm{a,void}}) = 0.965 C_{\mathrm{a0}}$ (The origin of the failure threshold will be explained in Section IV-A of this article), the failure of the atom was determined. The structure was reconstructed until the total atomic concentration fell below the threshold, and the total failure time was determined. Additionally, we compared the failure time obtained using the traditional atomic flux divergence method. The specific EM simulation process is shown in Fig. 3.

This study used the coefficient partial differential equation module in COMSOL. Additionally, the EM heat source coupling module and the thermal expansion and temperature coupling module from the multiphysics module were selected. By accounting for interactions between different physical fields, complete coupling of multiple physical fields

Authorized licensed use limited to: TU Delft Library. Downloaded on June 02,2025 at 10:30:01 UTC from IEEE Xplore. Restrictions apply.

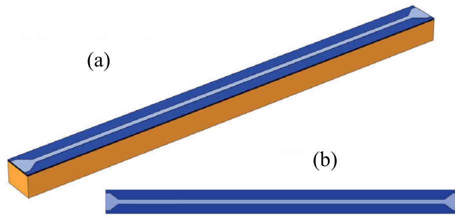

Fig. 4. (a) Three dimensional SWEAT-like model. (b) Top view.

TABLE II
PHYSICAL DESCRIPTIONS AND VALUES OF PARAMETERS USED IN THE EM SIMULATION [21], [22]

Parameters	Values*
Atomic concentration (C)	…m^{-3}
Local temperature (T)	…K
Time (t)	…K
Resistance (R)	…Ω
Atomic current density ($\mathbf{J}$)	…m^2/s
Current density vector ($\mathbf{j}$)	…MA/m^2
Diffusion coefficient (D_a)	…m^2/s
Hydrostatic stress (σ)	…Pa
Boltzmann constant (k)	1.38×10^{-23} J/K
Electron charge (e)	1.6×10^{-19} C
Initial atomic concentration (C_0)	1 mol/m^3
Effective charge number (Z*)	1
Heat of transport (Q*)	0.3 eV
Activation energy (E_a)	0.87 eV
Atomic volume (v)	1.66×10^{-29} m^3
Concentration for void formation ($C_{a,void}$)	0.965 C_0

TABLE III
RELATED PARAMETERS OF AL INTERCONNECT USED IN EM [21]

Parameter	Value
Poisson's ratio (v)	0.33
Electrical resistivity (ρ)	2.88×10^{-8} Ω×m
Temperature coefficient of resistivity	3.51×10^{-3} /K
Density	2700 Kg/m^3
Heat capacity	900 J/(Kg·K)
Thermal conductivity (k_m)	2.39 W/cm·K
Yield strength	200 − 0.35(T – 293 K) MPa

was achieved, and the model was calculated. This process involves computing the atomic flux driven by various forces and the atomic concentration in the interconnect at different times using finite element analysis. Accordingly, a 3-D model was developed to represent the Al interconnect circuits used in the experimental setup. As shown in Fig. 4(a), the heat dissipation gaskets at both ends were reduced in the simulation because they did not affect the distribution of the remaining experimental structure. The geometric dimensions of the EM process were consistent with the experimental results. The simulation was conducted under 3-D conditions and to present the changes more intuitively, a top-view perspective is used [Fig. 4(b)] in the subsequent illustrations. The parameters used in the EM simulation are listed in Tables II [22] and III [21].

IV. RESULTS AND DISCUSSION

In this section, the factors affecting EM are quantitatively analyzed, starting with four main driving forces and size

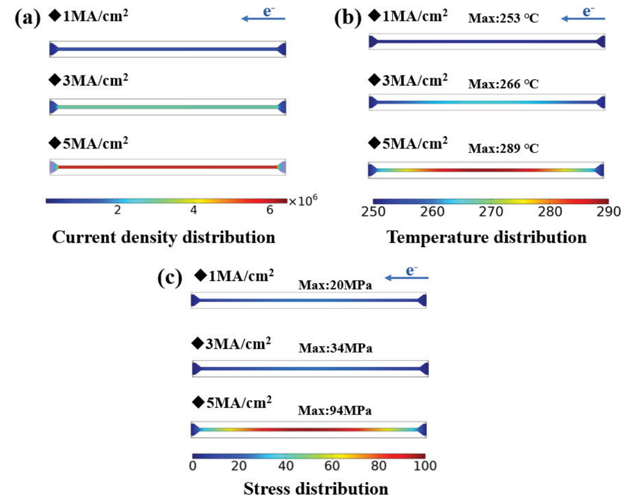

Fig. 5. (a) Current density, (b) temperature, and (c) stress distribution diagram of the Al SWEAT-like structure driven by different current densities.

factors. After removing the atoms below the void formation concentration in the SWEAT structure, the structure is reconstructed, and the EM failure lifetimes under three different current densities are calculated based on the relationship between atomic concentration and correlated resistivity. Finally, the simulation data obtained using the optimized method are compared with the experimental results and those obtained from the traditional atomic flux divergence method.

A. Current Density Effect on EM

As being driven by the current densities from 1 to 5 MA/cm^2, the current density, temperature, and stress distribution of the Al layer in the SWEAT structure are shown in Fig. 5.

First, Fig. 5(a) shows the distribution of current density in the Al layer, indicating that the maximum current density is concentrated in the narrowed part of the Al layer. The atomic flux at this maximum current density is the highest, resulting in the greatest number of atoms, which exacerbate EM failure and is most likely to lead to the formation of voids in the interconnect. However, voids were observed near the middle of the Al layer during the experiment. This indicates that other driving forces also influence failure in the EM process, and the location of the void cannot be accurately predicted using only the current density distribution. Next, Fig. 5(b) presents the temperature distribution in the Al layer, showing that the highest temperature of the Al interconnect occurs in the middle of the straight-line segment, while temperatures on both sides of the interconnect drop rapidly. Under the large liner, the temperature decreases to ambient levels. Due to the Joule effect, when current passes through the Al layer, it generates a significant amount of Joule heat, increasing the temperature of the Al layer. With a higher temperature, the atomic diffusion rate increases, resulting in maximum diffusion kinetic energy that accelerates atomic migration and raises the likelihood of void formation. Furthermore, Fig. 5(c) shows the von Mises stress distribution in the Al layer. Due to the differences in

Authorized licensed use limited to: TU Delft Library. Downloaded on June 02,2025 at 10:30:01 UTC from IEEE Xplore. Restrictions apply.

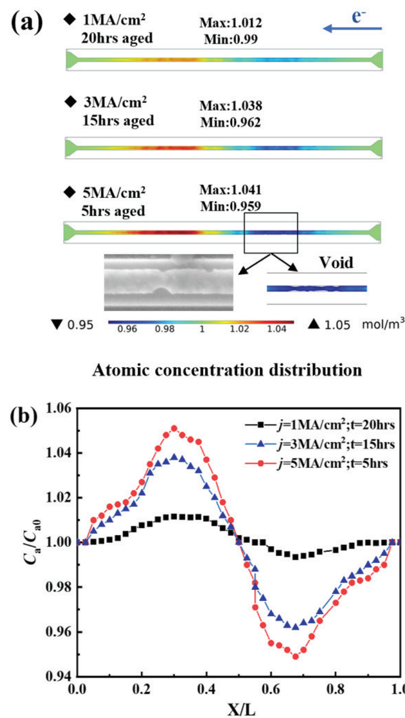

Fig. 6. Atomic concentration distribution under different current densities and aging times. (a) Cloud map. (b) C_a/C_{a0} along the length.

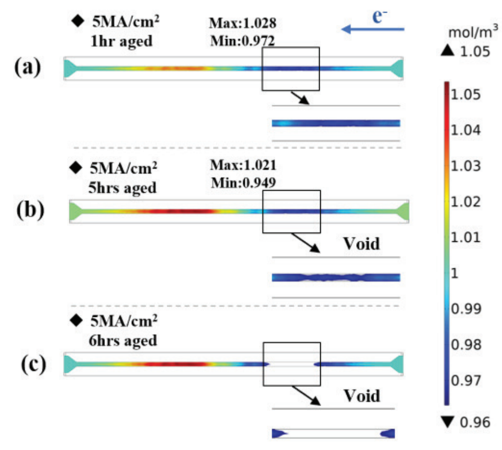

Fig. 7. Atomic concentration distribution after it reached the failure threshold at a current density of 5 MA/cm^2: (a) 1; (b) 5; and (c) 6 h of aging.

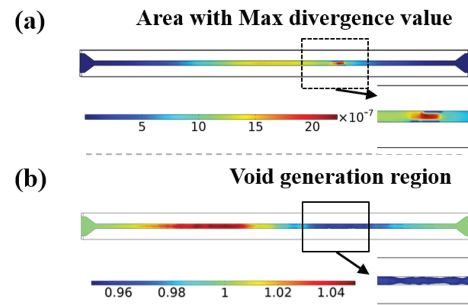

Fig. 8. Atomic flux divergence distribution and voids in the interconnects. [Calculated based on (14)]. (a) Atomic flux divergence distribution. (b) Voids in the interconnects.

geometric size between the Al and Si layers, there is no continuous connection, and the thermal expansion coefficients of the two layers differ. Under the influence of Joule heat, the two layers exert pressure on each other, causing stress. The maximum stress in the Al layer is primarily concentrated in the middle of the straight-line segment. This uneven stress distribution leads to a stress gradient in the Al layer, and the migration of tension atoms along the direction of this stress gradient contributes to stress migration.

The failure of the Al layer was analyzed based on the distribution of current density, temperature, and stress. Unfortunately, the location of voids in the Al interconnect cannot be accurately predicted. The atomic concentration distributions of the Al layer in the SWEAT-like structure after EM are shown in Fig. 6. The maximum atomic concentration in the Al layer occurs in the middle-left position, while the minimum atomic concentration is found in the middle-right position of the straight-line segment of the Al layer, which is consistent with the experimental results. At the minimum atomic concentration, the atomic outflow is the largest, most likely causing mass transfer.

In the work of Cui et al. [22], the void length and atomic drift velocity of the SWEAT structure were obtained under experimental conditions of 250 °C and a current density of 1 MA/cm^2. Assuming that the decrease in atomic concentration of the void is equal to the increase in atomic concentration of the hillock, it is deduced that the concentration for void formation ($C_{a,\text{void}}$) = $0.965C_{a0}$. In this study, the failure threshold was set to 0.965 mol, meaning that the critical atomic density below which failure occurs is 0.965 mol. As the resistivity of the material increases with a decrease in atomic density, interconnect failure can be determined by whether the atomic concentration reaches the threshold corresponding to the change in resistance. After reaching the threshold, atomic accumulation will gradually decrease to 0.949 mol.

Fig. 7 shows the atomic concentration distribution and void changes over time under a current density of 5 MA/cm^2. It can be seen that the void generation velocity increases sharply after the void transitions from the formation stage to the expansion stage. With the continuous migration of atoms, the electrical conductivity of the unit with reduced atomic density will gradually decrease, leading to an increase in local current density. There is a maximum current density at which voids appear, and due to the effects of Joule heat, the temperature in that area will increase. The larger current density and temperature will further promote atomic migration speed, causing the interconnect to fail rapidly.

Fig. 8 shows the atomic flux divergence distribution and voids in the interconnects. When the current load is applied, the atoms in the interconnect migrate in the direction of the electron flow, and the nonuniformity of the concentration distribution increases over time. The atomic concentration in this region gradually increases as atoms accumulate near the anode, while atoms near the cathode substrate migrate away, leading to a gradual decrease in concentration in that area. Under the influence of atomic concentration redistribution, the geometric

Authorized licensed use limited to: TU Delft Library. Downloaded on June 02,2025 at 10:30:01 UTC from IEEE Xplore. Restrictions apply.

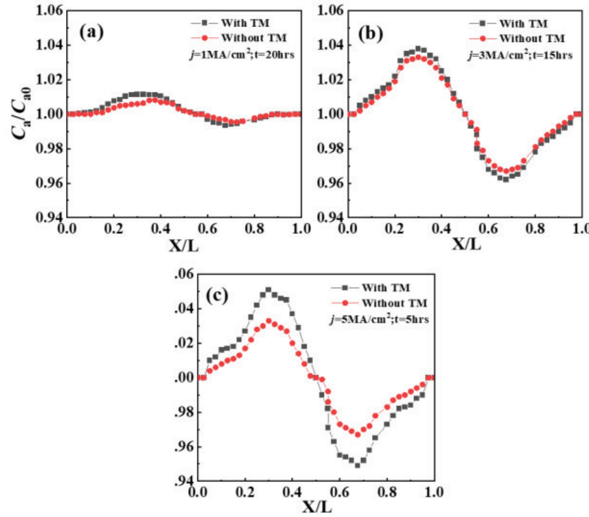

Fig. 9. C_a/C_{a0} along the length of SWEAT structure: (a) j = 1 MA/cm^2, t = 20 h; (b) j = 3 MA/cm^2, t = 15 h; and (c) j = 5 MA/cm^2, t = 5 h.

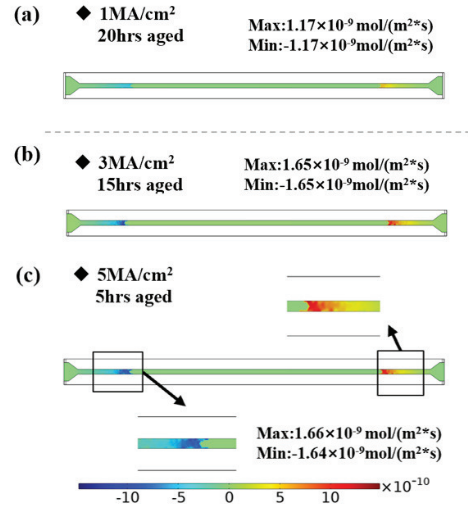

Fig. 10. Effect of stress transfer on EM increases with an increase in power-up time: (a) j = 1 MA/cm^2, t = 20 h; (b) j = 3 MA/cm^2, t = 15 h; and (c) j = 5 MA/cm^2, t = 5 h. [Calculated based on (5).]

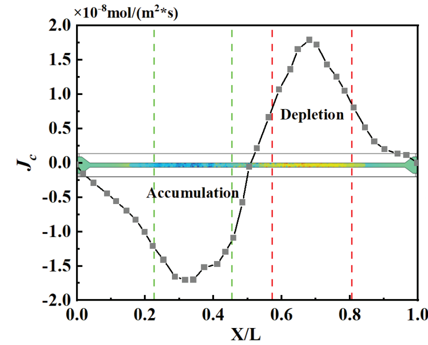

Fig. 11. Effect of atomic self-diffusion. [Calculated based on (6).]

shape of the structure changes, and voids are gradually formed. The maximum divergence of the total atomic flux corresponds to the region where void formation occurs in the simulation.

B. Thermal Transfer Effect on EM

Another macroscopic manifestation in the EM process of metal interconnects is the thermal effect inside the interconnects [23]. Fig. 9(a)–(c) shows the effect of thermal migration on the atomic migration of the interconnect under different current densities and time, respectively.

The concentration of atoms begins to change in regions near both boundaries due to the presence of a temperature gradient on either side, which triggers the diffusion of atoms away from the interconnect. By comparing the results, we found that heat transfer had no noticeable effect on atomic density under the condition of 1 MA/cm^2. In the steady state, C_a/C_{a0} remained stable at 20 h under the condition of 1 MA/cm^2. With the increase in current, the effect of thermal migration on atomic migration increased accordingly, the proportion of C_a/C_{a0} change is higher than 1 and 3 MA/cm^2 under the condition of 5 MA/cm^2. In summary, according to the analysis, for interconnects within integrated circuits, current density emerges as the primary determinant of the EM lifetime within a specific temperature range. However, as current density gradually increases, the contribution of thermal transfer to EM cannot be ignored.

C. Stress Transfer Effect on EM

The influence of stress migration on EM is shown in Fig. 10. There are significant differences in stress migration under the three different current densities. Under a current density of 1 MA/cm^2, the maximum stress transfer is 1.17×10^{-9} mol/(m$^2\times$ s), and under 3 MA/cm^2, the maximum stress transfer is 1.65×10^{-9} mol/(m$^2\times$ s). Compared to 3 MA/cm^2, the maximum stress transfer under 5 MA/cm^2 remains essentially unchanged. In the process of EM, atoms diffuse from the cathode toward the anode, propelled by the force exerted by electron wind. Additionally, many atoms accumulate at the anode, forming compressive stress, while the cathode experiences tensile stress. Therefore, a stress gradient from the anode to the cathode is created, affecting the migration of atoms, as illustrated in Fig. 10(c) [14]. Furthermore, due to the differences in thermal expansion coefficients between materials, such as those of Al and SiO_2, a nonuniform distribution of stress leads to stress migration. Since the temperature produced after the application of current density is higher than the initial temperature, the Al line releases only a portion of the elastic strain.

D. Atomic Self-Diffusion Effect on EM

The traditional atomic flux divergence method [32] ignores the influence of the atomic density gradient, which is addressed in this study. Fig. 11 shows that the atomic concentration flux divergence is inversely proportional to the total atomic flux divergence distribution. The atomic concentration gradient and stress gradient are the only two forces in EM that balance the electron wind force. This means that the atomic density gradient can inhibit EM and resist atomic loss and

Authorized licensed use limited to: TU Delft Library. Downloaded on June 02,2025 at 10:30:01 UTC from IEEE Xplore. Restrictions apply.

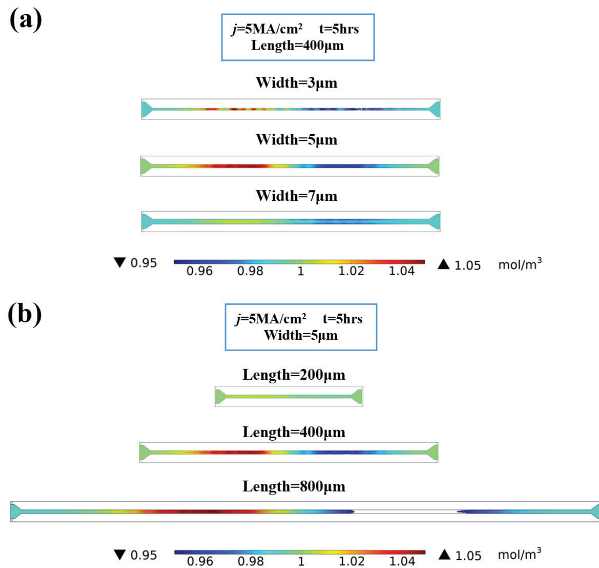

Fig. 12. (a) Effect of interconnect width. (b) Effect of interconnect length on EM (j = 5 MA/cm^2, t = 5 h).

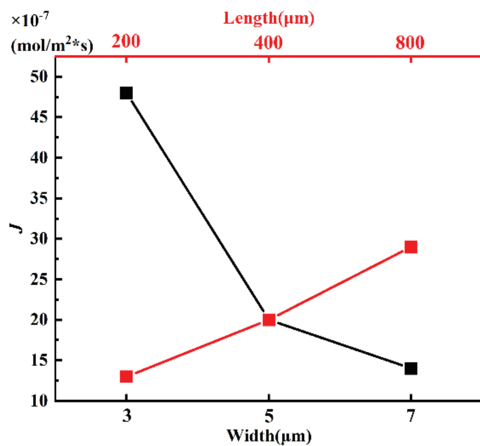

Fig. 13. Relationship between the maximum atomic flux and the length and width of Al interconnect.

void expansion. Therefore, if the atomic density gradient is not considered, the EM failure lifetime will be underestimated.

E. Interconnect Size Effect on EM

In this section, current density loads of 5 MA/cm^2 were applied to SWEAT-like structure models with different lengths and widths of Al interconnects, and the internal atomic flux distributions were obtained. The atomic concentrations at varying lengths and widths are shown in Fig. 12.

The relationship between the maximum atomic flux and the length and width of the Al interconnect is shown in Fig. 13. As seen in Fig. 13, the general trend indicates that the atomic flux inside the interconnect decreases gradually with an increase in the width of the Al interconnect, with a sharp decrease occurring in the initial stage (when the width increases from 3 to 5 μm). This trend suggests that when the width of the interconnect is 5 μm or less, the probability of interconnect failure will significantly increase. Conversely, as

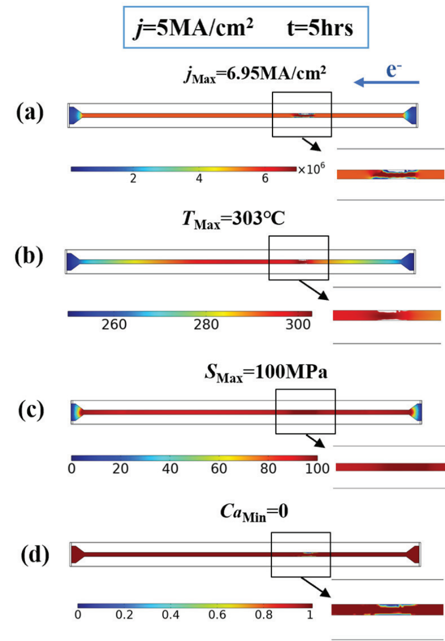

Fig. 14. (a) Current density, (b) temperature, (c) stress, and (d) atomic concentration distribution after structural reconstruction.

the length of the Al interconnect increases, the atomic flux inside the interconnect gradually increases, which is more likely to produce voids and atomic accumulation, accelerating EM failure.

F. EM Failure Criterion and Lifetime Prediction

Under static analysis conditions, it is assumed that there are no voids in the analysis, and the current, temperature distribution, and stress distribution remain unchanged throughout the process. Thus, the model does not need to be reconstructed, and the location of the simulated voids is consistent with the experimental results. To account for the effect of atomic concentration migration, we deleted the atoms below the threshold and reconstructed the structure, as shown in Fig. 14. The reconstructed structure can be energized normally. As atoms continue to migrate, the electrical conductivity of the unit with reduced atomic density will gradually decrease, resulting in an increase in local current density. Fig. 14(a) shows the current density distribution at the point of EM failure. The maximum current density occurred at the location of the void and increased from the original 5 to 6.95 MA/cm^2 at failure. Due to Joule heating, the temperature also increased, as shown in Fig. 14(b). The maximum temperature reached 303 °C, which is significantly higher than the initial temperature of 250 °C. The structural stress also increased. With higher-current density, temperature, and stress, the migration speed of atoms will further accelerate, resulting in faster EM failure.

The damage degradation caused by the growth and merging of EM voids in the interconnect extends throughout the stress area of the interconnect, representing a gradual deterioration process from the onset of deformation to failure [36]. With the coupling of multiple field loads, the damage involves a quantitative accumulation process leading to failure. In this

Authorized licensed use limited to: TU Delft Library. Downloaded on June 02,2025 at 10:30:01 UTC from IEEE Xplore. Restrictions apply.

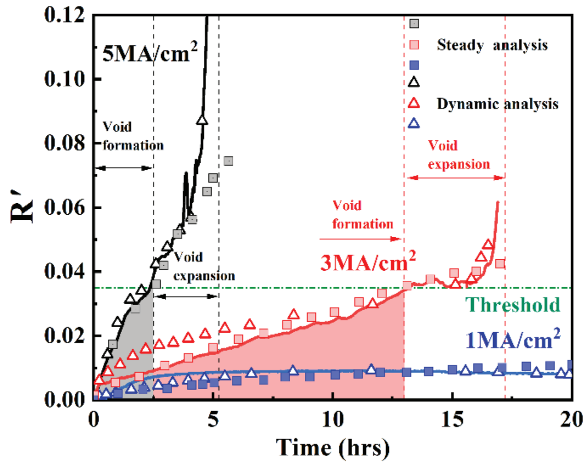

Fig. 15. Evolution of the resistance before and after reaching the threshold of void formation (i.e., the atomic concentration decreased to 0.965 mol) at different current densities (the solid line represents the experimental results, and the scatter plot is the simulation result) [21].

process, the existence, development, and evolution of damaged elements result in the actual materials and structures being neither homogeneous nor continuous.

Due to the continuous directional movement of atoms in the EM process, local lattice vacancies will occur when the migration velocity of the atoms does not match that of the lattice, leading to the formation of macroscopic voids. This phenomenon impacts the material properties. In this study, we consider the continuous changes in resistivity and material properties throughout the atomic migration process. The formula for calculating the resistance of the material is as follows [25]:

$$R = \rho \frac{V}{s} \tag{16}$$

where V and s are the cross-sectional and effective cross-sectional areas of the interconnect, respectively. The cross section refers to the normal cross-sectional area of an aluminum wire, while the effective cross section refers to the area reduction caused by atomic loss during EM. When the cross-sectional area is constant, the resistance is inversely proportional to the effective cross-sectional area, which arises due to the migration of atoms. Material defects, such as voids, will reduce the cross-sectional area of the conductive channel. We can consider the regularized atomic density as the measure of damage, and thus, the degree of reduction in the effective cross-sectional area can be expressed as follows:

$$s' = sC_{\mathrm{a}}. \tag{17}$$

Therefore, with a decrease in atomic density, the resistance change is as follows:

$$R' = \rho \frac{V}{s'} = \rho \frac{V}{sC_{\mathrm{a}}} = \rho(C_{\mathrm{a}}) \frac{V}{s}. \tag{18}$$

The formation of interface voids in interconnects will increase the resistance of the interconnect, which is often the cause of the decrease in cross section and the local temperature increase at the point of interconnect failure. The moment when the hollow electrical contact at the interface is destroyed (resulting in a sudden sharp increase in interface resistance) is referred to as the failure time [time to failure (TTF)]. Fig. 15 and Table IV show that the simulation results align closely with the experimental results. In the steady-state analysis, due to the inhibition of the atomic concentration gradient, the atomic concentration changes from rapidly decreasing to saturation over time. Compared to the steady-state analysis, the dynamic simulation shows little difference during the void formation stage. After determining the failure (void expansion stage), we found that the model based on the improved atomic flux divergence method better matches the resistance change curve, reducing the failure time error by about 10%.

TABLE IV

COMPARISON OF FAILURE TIMES FROM THE EXPERIMENT WITH THOSE CALCULATED USING TWO DIFFERENT SIMULATION SETTINGS

Item	Experimental results	Predicted results with traditional atomic flux divergence method (Static analysis)	Predicted results with improved atomic flux divergence method (Dynamic analysis)
TTF - 3MA/cm² (h)	15.91	14.04	15.78
TTF - 5MA/cm² (h)	2.44	2.68	2.38

V. CONCLUSION

In this article, the SWEAT-like structures are tested under different current densities (1, 3, and 5 MA/cm^2). Based on FEM and the atomic flux divergence method, we proposed a simulation method for the EM acceleration of electronic devices under 3-D multiphysical field coupling to quantitatively analyze the contributions of current density, temperature, stress, and self-diffusion to EM. After deleting the atoms below the threshold, the structure was reconstructed and dynamically analyzed. Finally, the prediction of the failure lifespan was executed and subsequently compared with the findings obtained through experimental validation and the traditional atomic flux divergence approach.

The results showed the following.

1) Changes in current density could directly affect the EM failure mode in the SWEAT-like interconnect structure. Under higher-current conditions, Al atoms were more likely to migrate. The contribution of the temperature gradient was limited at 1 MA/cm^2, while its effect on atomic diffusion increased with the increase in current density. The atomic concentration gradient and stress gradient could inhibit EM failure, and ignoring them would underestimate the failure life of EM.
2) Structural size was also a key factor affecting the failure life of EM. An increase in the length and a decrease in the width of the Al interconnect both led to a gradual increase in atomic flux inside the interconnect, making the structure more prone to atomic diffusion and accumulation, thereby accelerating EM failure.
3) Changes in atomic flux and atomic concentration showed opposite trends. We described the development process of EM as consisting of a void formation stage and

Authorized licensed use limited to: TU Delft Library. Downloaded on June 02,2025 at 10:30:01 UTC from IEEE Xplore. Restrictions apply.

a void expansion stage. The improved method better fit the changing trend of atomic concentration after interconnect failure and predicted the accelerated EM failure time more accurately during the void expansion stage, reducing the failure time error by about 10%.

In this article, Al was chosen as the carrier material for the EM study; however, the theoretical framework and experimental methodologies presented herein have the potential for broader application to diverse interconnect material systems in the realm of micro- and nanoelectronics, including materials such as copper (Cu) or gold (Au). In future work, we plan to verify the universality and sensitivity of this method on other interconnect materials and structures and propose a more universal model for predicting the failure time of interconnect EM, which can provide a basis for the design, manufacture, and parameter optimization of the packaging process for microelectronic chips.

REFERENCES

[1] Y. Yang, L. Dorn-Gomba, R. Rodriguez, C. Mak, and A. Emadi, "Automotive power module packaging: Current status and future trends," *IEEE Access*, vol. 8, pp. 160126–160144, 2020.

[2] D. Straubinger, T. Hurtony, and A. Géczy, "Impact of electromigration and isothermal ageing on lead-free solder joints of chip-sized SMD components," *J. Mater. Res. Technol.*, vol. 21, pp. 308–318, Nov. 2022.

[3] M. N. Bashir et al., "Effect of zn nanoparticle-doped flux on mechanical properties of SAC305 solder joint after electromigration," *J. Mater. Sci., Mater. Electron.*, vol. 34, no. 4, p. 321, Feb. 2023.

[4] H. Ceric, H. Zahedmanesh, and K. Croes, "Analysis of electromigration failure of nano-interconnects through a combination of modeling and experimental methods," *Microelectron. Rel.*, vols. 100–101, Sep. 2019, Art. no. 113362.

[5] Z. Jin, F. Huo, J. Wang, X. Liu, Y. C. Chan, and H. Nishikawa, "Electromigration-induced microstructure evolution and failure mechanism of sintered nano-Ag joint," *Mater. Characterization*, vol. 205, Nov. 2023, Art. no. 113309.

[6] W. Li and C. M. Tan, "Black's equation for today's ULSI interconnect electromigration reliability—A revisit," in *Proc. IEEE Int. Conf. Electron Devices Solid-State Circuits*, Nov. 2011, pp. 1–2.

[7] Y. Wang, B. Li, Y. Zhifeng, and Y. Yao, "Interfacial fracture caused by electromigration at copper interconnects," *J. Electron. Packag.*, vol. 146, no. 1, Mar. 2024, Art. no. 011007.

[8] C.-H. Chen, P.-I. Lee, and T.-H. Chuang, "Microstructure evolution and failure mechanism of electromigration in Ag-alloy bonding wire," *J. Alloys Compounds*, vol. 913, Aug. 2022, Art. no. 165266.

[9] C. Dong and P. Huang, "Finite element simulation of inclusion evolution in interconnects due to electromigration-induced interface diffusion," *Arch. Appl. Mech.*, vol. 93, no. 3, pp. 1081–1094, Mar. 2023.

[10] F. Wolff, D. Weyer, C. Papachristou, and S. Clay, "Design for reliability: Tradeoffs between lifetime and performance due to electromigration," *Microelectron. Rel.*, vol. 117, Feb. 2021, Art. no. 114025.

[11] C.-L. Liang et al., "Athermal and thermal coupling electromigration effects on the microstructure and failure mechanism in advanced fine-pitch Cu interconnects under extremely high current density," *Mater. Chem. Phys.*, vol. 256, Dec. 2020, Art. no. 123680.

[12] Y. Zhang, Y. Liu, L. Liang, and X. Fan, "The effect of atomic density gradient in electromigration," *Int. J. Mater. Struct. Integrity*, vol. 6, no. 1, p. 36, 2012.

[13] C. Basaran, "Unified mechanics of metals under high electrical current density: Electromigration and thermomigration," in *Introduction to Unified Mechanics Theory With Applications*. Cham, Switzerland: Springer, 2022, pp. 427–458.

[14] I. A. Blech and K. L. Tai, "Measurement of stress gradients generated by electromigration," *Appl. Phys. Lett.*, vol. 30, no. 8, pp. 387–389, Apr. 1977.

[15] I. A. Blech and C. Herring, "Strss generation by electromigration," *Appl. Phys. Lett.*, vol. 29, no. 3, pp. 131–133, 1976.

[16] I. A. Blech, "Electromigration in thin aluminum films on titanium nitride," *J. Appl. Phys.*, vol. 47, no. 4, pp. 1203–1208, 1976.

[17] M. A. Korhonen, P. Børgesen, K. N. Tu, and C.-Y. Li, "Stress evolution due to electromigration in confined metal lines," *J. Appl. Phys.*, vol. 73, no. 8, pp. 3790–3799, 1993.

[18] J. J. Clement and C. V. Thompson, "Modeling electromigration-induced stress evolution in confined metal lines," *J. Appl. Phys.*, vol. 78, no. 2, pp. 900–904, Jul. 1995.

[19] M. E. Sarychev, Y. V. Zhitnikov, L. Borucki, C.-L. Liu, and T. M. Makhviladze, "A new, general model for mechanical stress evolution during electromigration," *Thin Solid Films*, vol. 365, no. 2, pp. 211–218, Apr. 2000.

[20] R. J. Gleixner, B. M. Clemens, and W. D. Nix, "Void nucleation in passivated interconnect lines: Effects of site geometries, interfaces, and interface flaws," *J. Mater. Res.*, vol. 12, no. 8, pp. 2081–2090, Aug. 1997.

[21] Z. Cui, X. Fan, and G. Zhang, "General coupling model for electromigration and one-dimensional numerical solutions," *J. Appl. Phys.*, vol. 125, no. 10, Mar. 2019, Art. no. 105101.

[22] Z. Cui, X. Fan, Y. Zhang, S. Vollebregt, J. Fan, and G. Zhang, "Coupling model of electromigration and experimental verification—Part I: Effect of atomic concentration gradient," *J. Mech. Phys. Solids*, vol. 174, May 2023, Art. no. 105257.

[23] Z. Cui, X. Fan, Y. Zhang, S. Vollebregt, J. Fan, and G. Zhang, "Coupling model of electromigration and experimental verification—Part II: Impact of thermomigration," *J. Mech. Phys. Solids*, vol. 174, May 2023, Art. no. 105256.

[24] S.-W. Chen et al., "Effects of electromigration on electronic solder joints," in *Lead Free Solders: Materials Reliability for Electronics*, 2012, pp. 401–422. [Online]. Available: https://onlinelibrary.wiley.com/doi/pdf/10.1002/9781119966203.ch16

[25] X. Chen, L. Liang, and Y. Liu, "Electromigration simulation with consideration of the atomic concentration gradient," in *Proc. Int. Conf. Electron. Packag. Technol. High Density Packag.*, Jul. 2008, pp. 1–7.

[26] P.-T. Lee, C.-Y. Lee, W.-Z. Hsieh, C.-T. Chen, and C.-E. Ho, "Electromigration-induced remarkable intermetallic compound (IMC) formation in micro joints and its prevention," *J. Mater. Res. Technol.*, vol. 24, pp. 3889–3900, May 2023.

[27] H. Ceric, R. L. de Orio, and S. Selberherr, "Statistical study of electromigration in gold interconnects," *Microelectron. Rel.*, vol. 147, Aug. 2023, Art. no. 115061.

[28] Z. Shen, S. Jing, Y. Heng, Y. Yao, K. N. Tu, and Y. Liu, "Electromigration in three-dimensional integrated circuits," *Appl. Phys. Rev.*, vol. 10, no. 2, Jun. 2023, Art. no. 021309.

[29] H. Tian et al., "Thermoreflectance imaging of electromigration evolution in asymmetric aluminum constrictions," *J. Appl. Phys.*, vol. 123, no. 3, Jan. 2018, Art. no. 035107.

[30] Z. Wang, S. Alajlouni, P. Bermel, and A. Shakouri, "Explaining an unusual electromigration behavior—A comprehensive experimental and theoretical analysis using finite element method," *J. Appl. Phys.*, vol. 129, no. 21, Jun. 2021, Art. no. 214502.

[31] M. Kato, T. Omori, A. Goryu, T. Fumikura, and K. Hirohata, "Electromigration analysis of solder joints for power modules using an electrical-thermal-stress coupled model," *J. Electron. Packag.*, vol. 144, no. 2, Aug. 2021, Art. no. 021102.

[32] K. Sasagawa, M. Hasegawa, M. Saka, and H. Abé, "Atomic flux divergence in bamboo line for predicting initial formation of voids and hillocks," *Theor. Appl. Fract. Mech.*, vol. 33, no. 1, pp. 67–72, Feb. 2000.

[33] C. M. Tan, G. Zhang, and Z. Gan, "Dynamic study of the physical processes in the intrinsic line electromigration of deep-submicron copper and aluminum interconnects," *IEEE Trans. Device Mater. Rel.*, vol. 4, no. 3, pp. 450–456, Sep. 2004.

[34] X. Zhao, Y. Kimura, and M. Saka, "Analyzing electromigration near a right-angled corner composed of dissimilar metals by investigating the effect of material combination on atomic flux divergence," *Jpn. J. Appl. Phys.*, vol. 53, no. 7, Jul. 2014, Art. no. 075504.

[35] Z. Guan, M. Marek-Sadowska, S. Nassif, and B. Li, "Atomic flux divergence based current conversion scheme for signal line electromigration reliability assessment," in *Proc. IEEE Int. Interconnect Technol. Conf.*, May 2014, pp. 245–248.

[36] S.-K. Lin, Y.-C. Liu, S.-J. Chiu, Y.-T. Liu, and H.-Y. Lee, "The electromigration effect revisited: Non-uniform local tensile stress-driven diffusion," *Sci. Rep.*, vol. 7, no. 1, p. 3082, Jun. 2017.

Authorized licensed use limited to: TU Delft Library. Downloaded on June 02,2025 at 10:30:01 UTC from IEEE Xplore. Restrictions apply.